Published in final edited form as:
Bioconjug Chem. 2011 April 20; 22(4): 709–716. doi:10.1021/bc100464e.

SITE SPECIFIC CONJUGATION OF MONODISPERSED DOTA-PEGn TO THIOLATED DIABODY REVEALS EFFECT OF INCREASING PEG SIZE ON KIDNEY CLEARANCE AND TUMOR UPTAKE WITH IMPROVED 64-COPPER PET IMAGING

Lin Li[1,*], **Desiree Crow**[3,*], **Fabio Turatti**[2,*], **James R. Bading**[3], **Anne-Line Anderson**[3], **Erasmus Poku**[3], **Paul J. Yazaki**[3], **Jenny Carmichael**[2], **David Leong**[2], **Michael P. Wheatcroft**[2], **Andrew A. Raubitschek**[3], **Peter J. Hudson**[2,#], **David Colcher**[3,#], and **John E. Shively**[1,4,#]

[1]Department of Immunology, Beckman Research Institute of City of Hope, Duarte, CA 91010

[2]Avipep Pty Ltd, 343 Royal Parade, Parkville VIC 3008, Australia

[3]Department of Cancer Immunotherapeutics & Tumor Immunology, Beckman Research Institute of City of Hope, Duarte, CA 91010

Abstract

Optimal PET imaging of tumors with radiolabeled engineered antibodies requires, among other parameters, matching blood clearance and tumor uptake with the half-life of the engineered antibody. Although diabodies have favorable molecular sizes (50 kDa) for rapid blood clearance ($t_{1/2}$= 30-60 min) and are bivalent, thereby increasing tumor uptake, they exhibit substantial kidney uptake as their major route of clearance, which is especially evident when they are labeled with the PET isotope ^{64}Cu ($t_{1/2}$= 12 hr). To overcome this drawback, diabodies may be conjugated to PEG, a modification that increases the apparent molecular size of the diabody and reduces kidney uptake without adversely affecting tumor uptake or the tumor to blood ratio. We show here that site specific attachment of monodispersed PEGn of increasing molecular size (n= 12, 24, and 48) can uniformly increase the apparent molecular size of the PEG-diabody conjugate, decrease kidney uptake and increase tumor uptake, the latter due to the increased residence time of the conjugate in the blood. Since the monodispersed PEGs were pre-conjugated to the chelator DOTA, the conjugates were able to bind radiometals such as ^{111}In and ^{64}Cu that can be used for SPECT and PET imaging, respectively. To allow conjugation of the DOTA-PEG to the diabody, the DOTA-PEG incorporated a terminal Cysteine conjugated to a vinyl sulfone moiety. In order to control the conjugation chemistry, we have engineered a surface thiolated diabody that incorporates two cysteines per monomer (four per diabody). The thiolated diabody was expressed and purified from bacterial fermentation and only needs to be reduced prior to conjugation to the DOTA-PEGn-Cys-VS. This novel imaging agent (a diabody with DOTA-PEG48-Cys-VS attached to introduced thiols) gave up to 80 %ID/g of tumor uptake with a tumor to blood ratio (T/B) of 8 at 24h when radiolabeled with ^{111}In and 37.9% ID/g of tumor uptake (T/B= 8) at 44h when radiolabeled with ^{64}Cu in PET imaging in an animal model. Tumor uptake was significantly improved from the 50% ID/g at 24 hours observed with diabodies that were pegylated on surface Lysine residues. Importantly, there was no loss of immunoreactivity of the site-specific Cys-conjugated diabody to its antigen (TAG-72) compared to the parent, unconjugated diabody. We

[4]To whom correspondence should be addressed J.E. Shively, Tel: 626-359-8111 ext 62601, jshively@coh.org.
[*]These authors contributed equally to this research.
[#]Equal contribution of senior authors.

propose that thiolated diabodies conjugated to DOTAylated monodisperse PEGs have the potential for superior SPECT and PET imaging in a clinical setting.

Keywords

Diabody; CC49; TAG-72; DOTA; Cu-64; polyethylene glycol; PET

INTRODUCTION

Optimal PET imaging of tumors with radiolabeled engineered antibodies requires, among other parameters, matching blood clearance and tumor uptake with the half-life of the engineered antibody (1, 2). Although diabodies have favorable molecular sizes (50 kDa) for rapid blood clearance ($t_{1/2}$= 30-60 min) and are bivalent increasing tumor uptake, they exhibit substantial kidney uptake as their major route of clearance, which is especially evident when they are labeled with the PET isotope ^{64}Cu ($t_{1/2}$= 12 hr). To overcome this drawback, diabodies may be conjugated to PEG, a modification that increases the apparent molecular size of the diabody and reduces kidney uptake without adversely affecting tumor uptake or the tumor to blood ratio (3). Recently, we have shown monodispersed PEGs, as opposed to polymeric PEGs, can not only achieve this goal, but also can incorporate bifunctional chelators such as DOTA to allow preparation of a conjugate ready for radiolabeling with a variety of radiometals (4). In that study, we synthesized a number of monodispersed PEGs of different sizes starting from FMOC-NH-PEGn-COOH (where n= 12, 24, 24, and 48) that had DOTA at the “amino-” terminus and Cysteine at the “carboxy-” terminus using a standard solid phase peptide synthesis approach. The product DOTA-NH-PEGn-Cys, which had a free thiol was derivatized with vinyl sulfone, yielding a product that could be conjugated to proteins by Michael addition to either thiol or amino groups by control of the pH (5). Since the starting diabody had no surface thiol groups, all of the conjugations were made to surface amino groups. Although, we were successful in demonstrating the principle that addition of monodispersed PEG could favorably modify the diabody improving biodistributions and subsequent imaging, this approach does not allow a precise control of the addition of the PEG conjugates and may not be generally applicable to diabodies where over-conjugation with PEG to amino groups may lead to decreased immunoreactivity.

A potential solution to this problem has been proposed by a number of groups through incorporation of site-specific amino acid replacements to add surface thiol residues into intact antibodies. This included the recent study by Tinianow et al. (6) who generated a thiolated MAb that was site specific conjugated to a maleimido-desferrioxamine and radiolabeled with ^{89}Zr for PET imaging. In that study the half-life of the radiolabel ($t_{1/2}$= 4d) was well-matched with the blood clearance of an intact MAb ($t_{1/2}$= 2-3d). However, as noted by Janutula et al. (7), most single-site cysteine additions result in intermolecular aggregation, variable conjugation and result in poor expression yield for large scale processing. Furthermore, intact antibodies that were conjugated onto cysteine residues by partial reduction of interchain-disulfide bonds had variable stoichiometry (zero to eight drugs per antibody) and potentially yielded >100 species (7). For diabodies, both additional C-terminal cysteine residues (8) and intra-chain disulfides (9) have been designed, although production yields were low.

In this manuscript, we designed a stable intra-domain disulfide bond in a surface-exposed region of the L1 loop in the VL domain of an anti-TAG-72 diabody. Molecular modeling ensured the two cysteine residues were about 6-7 Å apart and positioned so that their side chain thiol groups were exposed to solvent and could form a disulfide bond. This resulted in

a stable, well-folded diabody, produced by bacterial expression and which could be reduced and conjugated to our previously described DOTA-NH-PEGn-Cys-VS where n= 12, 24, and 48 at pH 7, a pH where the Michael addition reaction is specific for thiols. The resulting conjugates exhibited an average substitution of 3 PEGs per dimeric diabody out of a theoretical maximum of 4 PEGs per diabody. When studied in a mouse xenograft model, the three conjugates exhibited a monotonic decrease in kidney uptake in the order of n= 0, 12, 24, and 48, with n=48 giving the least kidney uptake (15 %ID/g at 4-72h) and the highest tumor uptake (80 %ID/g at 24-72h). The series also gave a monotonic increase in blood clearance in the order of n= 0, 12, 24, and 48, with n= 0 giving a blood clearance of $t_{1/2}$= 0.5h, and n=48 a blood clearance of $t_{1/2}$= 6.0h. Thus, it appears possible to fine-tune the biodistribution properties of a thiolated diabody with site specific conjugation of monodispersed PEGs. Since the n= 48 conjugate had the lowest kidney uptake, the highest tumor uptake, and an acceptable tumor to blood ratio (T/B= 8), this conjugate was radiolabeled with ^{64}Cu (half life well matched to blood clearance) and subjected to PET imaging in the mouse xenograft model. The resulting PET image was excellent in terms of tumor to blood contrast (T/heart = 8) with minimal imaging of other organs including the kidney and liver.

EXPERIMENTAL PROCEDURES

Materials, radiolabels, mass spectrometry

LS-174T cells were obtained from ATCC and maintained as previously described (10). 1,4,7,10-Tetraazacyclododecane-1,4,7-tris(*t*-butyl acetate)-10-acetic acid was obtained from Macrocyclics, Inc., Dallas, TX. N-FMOC-amido-dPEG-12 (and -24) acid was purchased from Quanta Biodesign Ltd (Powell, OH). ^{111}In chloride was from Amersham, ^{64}Cu chloride from Washington University School of Medicine, St. Louis, MO. Mass spectra were recorded on an Agilent 6520 Q-TOF LC/MS.

Construction, cloning, expression and purification of the anti-TAG-72 diabody AVP04-50 from AVP04-07

The parent anti-TAG-72 diabody (AVP04-07) (4) was based on V-domains from the parent CC49 murine monoclonal antibody and derivative scFv fragments. The expression gene cassette had codons optimized for E. coli expression with the orientation V_H-V_L joined by a G_4S linker and included a C-terminal His_6 tail. Two cysteines were introduced by replacement of Pro at FR1-8 and Leu at FR1-11 in FR1 of the VL domain (Kabat numbering). This construct AVP04-50 was otherwise identical to the parent AVP04-07 except it contained two additional cysteine residues per scFv monomer (4 cysteines per diabody). Molecular modeling had shown that these two cysteine residues were about 6-7 Å apart and positioned such that their side chain thiol groups could form a disulfide bond and, since exposed to solvent, could be reduced and labeled. Methods for determining solvent exposure or solvent accessible surface area included the Shrake-Rupley algorithm and LCPO method (11). AVP04-50 was subcloned into *E. coli* BL21 (DE3)(F^- *ompT hsdS*$_B$(r_B^- m_B^-) *gal dcm* (DE3)) (Novagen) and produced in an 18L fermentor. Bacterial lysate cleared by centrifugation (16,000 × *g*, 30 min) and filtration at 0.45 μm was purified using a three-step procedure (HisTrap, HiTrap SP HP, and Superdex 75 prep chromatography) on an AKTA Purifier 10 (GE Healthcare, Uppsala, Sweden). In this respect, the introduction of surface thiols into the L1 loop of the VL domain resulted in a well-folded diabody that could be expressed and purified from bacterial cell culture with equivalent yields to those reported earlier for the parent, non-thiolated, AVP04-07 diabody (4).

Immunoreactivity

Binding of AVP04-50 to the TAG-72 antigen was determined using bovine submaxillary mucin (BSM, Aldrich-Sigma (St. Louis, MO) in a column shift assay (Superdex 200).

Synthesis of DOTA-PEGn-Cys-VS and Conjugation to AVP04-50

N-FMOC-amido-PEGn-acid (where n= 12 or 24) was coupled to Cys-polystyrene Wang resin, the FMOC removed, coupled to DO3AtBu-Acid, cleaved and purified by RP-HPLC, reacted with a 10 molar excess of vinyl sulfone and repurified by RP-HPLC. DOTA-PEGn-Cys-VS was reacted with reduced (10 molar excess of TCEP) AVP04-50 diabody in pH 7 PBS at a molar ratio of 50. PEG 48 was generated by coupling PEG24 twice followed by coupling DO3AtBu-Acid with the remaining steps identical as above. All conjugates were analyzed by mass spectrometry to determine their degree of substitution.

Radiolabeling of AVP04-50 and its conjugates

Radiometal labeling of DOTA-AVP04-50 was performed using $^{111}InCl_3$ (0.15 mBq/μg) or $^{64}CuCl_2$ (0.37 mBq/μg) as previously described (12). Radiolabeling yields were typically 70-90%. The radiolabeled material was purified on Superdex-75 or 200 columns.

LS-174T Xenograft Model

Female, athymic *nu/nu* mice (Charles River Laboratories), 6 – 8 weeks old, were injected with LS-174T cells (10^6) s.c. in the flank. After 10 days mice were injected i.v. with 150 kBq of ^{111}In-labelled AVP04-50 (2-6 μg of total protein) for biodistribution studies. Mice were euthanized at various time points: tumor, blood and major organs were collected, weighed and counted. Time-activity curves were corrected for radioactive decay and presented as percentage of injected dose/g tissue.

PET imaging

Tumor-bearing mice were injected i.v. with ^{64}Cu-labeled DOTA-diabody or DOTA-PEGn-diabody conjugate and imaged at 1, 4, 21-22 and 45-46 h with a small-animal PET scanner (microPET Model R4; Siemens/CTIMI, Knoxville, TN). Mice anesthetized with isoflurane, were scanned for 20 min for the 1 and 4 h time points, 45 min at 21-22 h and 60 min at 44-45 h. Data were sorted into two-dimensional sinograms using the Fourier rebinning method and corrected for intrascan radiodecay, detector non-uniformity and random coincidence noise. Images were reconstructed by the iterative three-dimensional ordered subsets expectation maximization (OSEM) method (2 iterations, 12 subsets), followed by a maximum a posteriori (MAP) algorithm (18 iterations) (13).

RESULTS

Generation and characterization *of AVP04-50 Diabody*

The parent anti-TAG-72 diabody (AVP04-07) (4) was based on V-domains from the parent CC49 murine monoclonal antibody and derivative scFv fragments. The expression gene cassette had codons optimized for E. coli expression with the orientation V_H-V_L joined by a G_4S linker and included a C-terminal His_6 tail. Two cysteines were introduced by replacement of Pro at FR1-8 and Leu at FR1-11 in FR1 of the VL domain (Kabat numbering). This construct AVP04-50 was otherwise identical to the parent AVP04-07 except it contained two additional cysteine residues per scFv monomer (4 cysteines per diabody). AVP04-50 diabody expressed in E. coli and purified by a three-step method eluted as a single species on gel filtration as a monodispersed dimer with an apparent molecular mass of 52.5 kDa. The overall yield was 50-75% with immunoreactivity >99% as judged by a column shift assay (data not shown).

Synthesis and biodistributions of DOTA-PEGn AVP04-50 conjugates

Commercially available monodispersed PEG building blocks were converted into heterobifunctional reagents using a solid phase peptide synthesis methodology. First, we synthesized DOTA-PEGn-Cys-VS derivatives where n= 12, 24, and 48 as summarized in Scheme 1. Second, we conjugated DOTA-PEGn-Cys-VS to surface thiols of reduced diabody at pH 7.0 at a molar ratio of 50:1 (5). The unconjugated and conjugated versions of AVP04-50 were characterized by mass spectrometry (Fig 1). The unconjugated AVP04-50 had one major and two minor peaks, the major one (m/z= 26822) corresponding to the expected mass including the His6 C-terminal tag, and a minor peak at m/z= 25,999 corresponding to the expected mass minus the His6 tag (a second minor peak corresponds to loss of the His6 tag and two additional amino acids). The mass spectra of the conjugates reveals the presence of both conjugated and unconjugated species demonstrating that the two cysteines per monomer are not fully substituted. However, since there are two monomers per diabody, the percent unsubstituted is reduced accordingly. Attempts to increase the degree of substitution by the use of higher reagent to diabody ratios revealed that no further substituion could be achieved. This result may indicate that the unconjugated species may have reformed their disulfide bonds and that the monoconjugated species may inhibit the addition of a second conjugate. The results may also indicate that the Michael addition reaction is incomplete under these reaction conditions. Nonetheless, a comparison of the spectra indicates a relatively uniform degree of substitution among the three conjugates with substantial levels for the 0, 1, and 2 levels of substitution. There is also evidence for a small amount of 3 substituents, perhaps due to a low level of reaction at surface amino groups.

The three conjugates and the unconjugated diabody (conjugated to DOTA) were radiolabeled with ^{111}In, purified by size exclusion chromatography, and subjected to biodistribution studies in athymic mice bearing LS-174T xenografts. The size exclusion chromatography profiles reveal an apparent shift to higher molecular size in the order of n= 0, 12, 24, and 48 for the PEG size corresponding to apparent molecular weights of 50 kDa, 60 kDa, 70 kda, and 80 kDa, respectively (Fig 2). We conclude that increase in size of the monodispersed PEG is responsible for the uniform increase in apparent size of the conjugates. In all cases immunoreactivity of the conjugates was >95% (data not shown). Three major observations can be made from the biodistribution results shown in Fig 3A-D. First, the kidney uptake is uniformly reduced in the order n= 0, 12, 24, and 48 according to PEG size. For n= 0, kidney uptake is highest at 24h with a value of 120 %ID/g, and lowest for n= 48 at 24h with a value of 15 %ID/g. This corresponds to an 8-fold reduction in kidney uptake. Higher n values for PEG were not tested due to their commercial unavailability and the fact that increasing blood clearance would eventually lead to diminishing returns. Our results are in agreement with the kidney threshold for protein clearance is about 70-80 kDa. Second, tumor uptake is uniformly increased in the order n= 0, 12, 24, and 48 according to PEG size. Thus, tumor uptake for n= 0 at 24h is 30 %ID/g, but rises to 80 %ID/g for n= 48 at 24h. Third, blood clearance uniformly decreased in the order n= 0, 12, 24, and 48 according to PEG size. For n= 0, the $t_{1/2}$ was about 0.5h and for n= 48 about 6h. The increase in blood clearance with n is expected to result in better absolute tumor uptake, but can decrease the utility of the imaging agent if the T/B ratio starts to approach 1. A clinical consequence is the need to wait longer times for optimal T/B ratios, along with the need to match the radioisotope half-life with the blood clearance time. In this respect, the T/B for n= 0 is about 30 at 24h and decreases to about 8 at 24h for n= 48. In spite of these differences, it should be possible to image as early as 8h for both conjugates; e.g., with the n= 0 conjugate, T/B= 6 at 8h, compared to the n= 48 conjugate where T/B= 4 at 8h. However, the high kidney uptake for the n= 0 conjugate and its reduced absolute tumor uptake compared to the

n= 48 conjugate clearly make the n=48 conjugate the best choice of imaging agent for both the 8h and 24h times.

^{64}Cu PET imaging of DOTA-PEG48 conjugate of AVP04-50

Based on the ^{111}In-biodistribution results above, we concluded that the best candidate for ^{64}Cu PET imaging would be the n= 48 conjugate. This conjugate was expected to produce good tumor images as early as 8h, reach a maximum of tumor uptake at 24-48h, and to have a very low kidney and blood background. Given the 12h half-life of ^{64}Cu, imaging longer than 48h is not feasible, especially in a clinical setting where large amounts of isotope would be required to extend imaging to longer time periods. When comparing the images of AVP04-50 with no PEG, PEG-12, PEG-24, and PEG-48, PEG-48 is the clear winner in terms of absolute tumor uptake and lowest kidney uptake across the time points measured (Fig 4) or interms of time-activity curves (Fig 5). As expected, PET imaging of ^{64}Cu-labeled DOTA-PEG48-AVP04-50 (Fig 4D) demonstrated modest tumor uptake by 4h and very high tumor uptake at 21h and 44h with very low backgrounds at the later time. The measured tumor uptake for the PEG48 conjugate was 37.9 %ID/g at 44 h with a tumor to blood ratio of 8 and a tumor to liver ratio of 4. Under these conditions of PET imaging there was no interference from kidneys. The ^{64}Cu-PET results are similar to those for the ^{111}In-labeled PEGn= 48 conjugate biodistribution study and suggest that choice of radiometal has little effect on the biodistribution, an observation we made previously for an anti-CEA diabody (10).

DISCUSSION

Although antibodies have become an important source of targeted therapies, their routine use as imaging agents has not been fully realized. Obstacles to achieving this goal include matching the blood clearance half-life of the antibody with the radioisotope, maximizing both the absolute tumor uptake and tumor to blood ratio, and minimizing uptake into non-target organs such as the liver and kidney. Although several obstacles have been addressed by engineering antibody fragments of different molecular sizes, many of these approaches have led to compromises such as increased T/B at the expense of decreased absolute tumor uptake for scFvs (14). In this respect, diabodies that maintain the bivalency of intact antibodies but have faster blood clearance, appear to be a good choice in terms of maintaining good T/B ratios and absolute tumor uptake (15-18). With the selection of the diabody as the best candidate for imaging, one is left with selecting the best radioisotope and imaging modality. In terms of the latter, PET imaging emerges as the best choice in terms of its inherent quantitative nature and its ability to render good images at tumor to tissue ratios as low as 2:1 (19). In terms of the former, the choice of best PET isotope depends strongly on matching the half-life with the blood clearance and consideration of non-target uptake. Two radiometals, namely ^{64}Cu and ^{89}Zr, stand out as good candidates for PET imaging because of their ease of preparation, uncomplicated decays, and adequate yield of positron emissions (19). In terms of matching half-lives with blood clearance, ^{64}Cu ($t_{1/2}$= 12h) is most appropriate for fast clearing diabodies, and ^{89}Zr ($t_{1/2}$= 4d) for slower clearing whole antibodies. However, their use is often offset by the tendency of their antibody conjugates to have high uptake in non-target organs. Alternatively, ^{124}I ($t_{1/2}$= 4d) has the attraction that it is rapidly metabolized in the liver and kidney, reducing the uptake in non-target organs (20). The chief drawback to the use of this isotope is reduced uptake in tumor due to uptake and metabolism in the tumor itself if the antibody is internalized.

Given these considerations we chose to optimize imaging using ^{64}Cu labeled diabodies realizing that non-target organ uptake, especially the kidney, required more work. The problem with kidney uptake is well-understood. The kidney is the major excretion route for proteins with a molecular size less than 70 kda. Although such proteins are filtered by the

kidney, they are re-absorbed in the tubules and subjected to rapid degradation and recycling of their constituent components, some returned to blood and some excreted into urine. In the case of radiometal conjugates, the chelate-metal complex is only slowly excreted and therefore accumulates in the kidney. There are at least two potential solutions to this problem, either blocking the initial uptake or raising the apparent molecular size of the protein above the kidney threshold. Unfortunately blocking kidney uptake requires administering high doses of amino acids such as lysine (21) and is never complete. Raising the apparent molecular size of the protein has become the most attractive approach in spite of the fact that this will also increase blood retention and reduce the T/B. Thus, to effectively optimize this approach, one must carefully analyze a series of proteins that uniformly assess the key parameters of blood clearance, absolute tumor uptake, and T/B.

In terms of the choice of diabody, we chose anti-TAG-72. The anti-TAG-72 antibody CC49 and a diabody derivative of CC49 have been previously described (22-25) and CC49 intact IgG has been used in many clinical studies (26-28), making CC49 a good choice for a comparative study. In order to uniformly increase the apparent molecular size of the diabody, we engineered two cysteines per monomer into L1 of the VL domain. Using an hexahistidine-tagged, *E. coli* produced version of the CC49 diabody, namely AVP04-50, we found that an absolute tumor uptake in the LS-174T mouse model at 24 h of 30 %ID/g, superior to that previously reported for a $(scFv)_2$ version of CC49 (4 %ID/g) (29).

PEG was chosen as the best approach for modifying the apparent molecular size of the diabody because of the extensive literature demonstrating its beneficial effects on preventing rapid blood clearance of other proteins (30). We chose monodispersed rather than polydispersed PEG because it was necessary to increase its size in discrete increments, modify its structure to allow attachment of DOTA for radiolabeling purposes, and attach a linker moiety for conjugation to the diabody. We chose vinyl sulfone as the linker because of its ability to undergo site-specific Michael addition to cysteines engineered into the diabody. In addition, we had previously shown that conjugation of DOTA-PEG-Cys-VS to amino groups in the anti-TAG-72 diabody dramatically improved tumor uptake and reduced kidney clearance (4). We now proceeded to improve our optimization of this imaging agent by systematically examining the effect of different PEG sizes when conjugated to a thiolated diabody in a site-specific manner.

The results were satisfying in that we observed a uniform decrease in kidney uptake with increasing PEG size and a uniform increase in tumor uptake with increasing PEG size without a substantial compromise in T/B. Based on the comparisons, we selected the PEG of n= 48 for the optimal imaging agent and demonstrated excellent PET images at 24-48h when DOTA-PEG48-diabody was radiolabeled with ^{64}Cu. Taken together, the stable production platform offered by antibody fragments (4), coupled to the advantages of site-specific (thiol-targeted) conjugation for radiolabels (this manuscript) and new data on thiol-targeted antibody-drug conjugations (31), now extends the clinical opportunities of diabodies from SPECT and PET tumor imaging to drug-loaded delivery vehicles for tumor therapy.

Acknowledgments

This research was supported by a research grant from Avipep Pty Ltd, 343 Royal Parade, Parkville VIC 3008, Australia. Avibody proteins were prepared and shipped by Harjit Khangura of Avipep. $^{64}CuCl_2$ was obtained from Washington University, St. Louis, MO under NIH grant R24CA86307.

References

1. Wu AM, Olafsen T. Antibodies for molecular imaging of cancer. Cancer J. 2008; 14:191–7. [PubMed: 18536559]
2. Williams LE, Wu AM, Yazaki PJ, Liu A, Raubitschek AA, Shively JE, Wong JY. Numerical selection of optimal tumor imaging agents with application to engineered antibodies. Cancer Biother Radiopharm. 2001; 16:25–35. [PubMed: 11279795]
3. Yang K, Basu A, Wang M, Chintala R, Hsieh MC, Liu S, Hua J, Zhang Z, Zhou J, Li M, Phyu H, Petti G, Mendez M, Janjua H, Peng P, Longley C, Borowski V, Mehlig M, Filpula D. Tailoring structure-function and pharmacokinetic properties of single-chain Fv proteins by site-specific PEGylation. Protein Eng. 2003; 16:761–70. [PubMed: 14600206]
4. Li L, Turatti F, Crow D, Bading JR, Anderson AL, Poku E, Yazaki PJ, Williams LE, Tamvakis D, Sanders P, Leong D, Raubitschek A, Hudson PJ, Colcher D, Shively JE. Monodispersed DOTA-PEG-conjugated anti-TAG-72 diabody has low kidney uptake and high tumor-to-blood ratios resulting in improved 64Cu PET. J Nucl Med. 51:1139–46. [PubMed: 20554731]
5. Li L, Tsai SW, Anderson AL, Keire DA, Raubitschek AA, Shively JE. Vinyl sulfone bifunctional derivatives of DOTA allow sulfhydryl- or amino-directed coupling to antibodies. Conjugates retain immunoreactivity and have similar biodistributions. Bioconjug Chem. 2002; 13:110–5. [PubMed: 11792185]
6. Tinianow JN, Gill HS, Ogasawara A, Flores JE, Vanderbilt AN, Luis E, Vandlen R, Darwish M, Junutula JR, Williams SP, Marik J. Site-specifically 89Zr-labeled monoclonal antibodies for ImmunoPET. Nucl Med Biol. 2010; 37:289–97. [PubMed: 20346868]
7. Junutula JR, Raab H, Clark S, Bhakta S, Leipold DD, Weir S, Chen Y, Simpson M, Tsai SP, Dennis MS, Lu Y, Meng YG, Ng C, Yang J, Lee CC, Duenas E, Gorrell J, Katta V, Kim A, McDorman K, Flagella K, Venook R, Ross S, Spencer SD, Lee Wong W, Lowman HB, Vandlen R, Sliwkowski MX, Scheller RH, Polakis P, Mallet W. Site-specific conjugation of a cytotoxic drug to an antibody improves the therapeutic index. Nat Biotechnol. 2008; 26:925–32. [PubMed: 18641636]
8. Sirk SJ, Olafsen T, Barat B, Bauer KB, Wu AM. Site-specific, thiol-mediated conjugation of fluorescent probes to cysteine-modified diabodies targeting CD20 or HER2. Bioconjug Chem. 2008; 19:2527–34. [PubMed: 19053310]
9. Kim KM, McDonagh CF, Westendorf L, Brown LL, Sussman D, Feist T, Lyon R, Alley SC, Okeley NM, Zhang X, Thompson MC, Stone I, Gerber HP, Carter PJ. Anti-CD30 diabody-drug conjugates with potent antitumor activity. Mol Cancer Ther. 2008; 7:2486–97. [PubMed: 18723494]
10. Li L, Yazaki PJ, Anderson AL, Crow D, Colcher D, Wu AM, Williams LE, Wong JY, Raubitschek A, Shively JE. Improved biodistribution and radioimmunoimaging with poly(ethylene glycol)-DOTA-conjugated anti-CEA diabody. Bioconjug Chem. 2006; 17:68–76. [PubMed: 16417253]
11. Carmichael JA, Power BE, Garrett TP, Yazaki PJ, Shively JE, Raubischek AA, Wu AM, Hudson PJ. The crystal structure of an anti-CEA scFv diabody assembled from T84.66 scFvs in V(L)-to-V(H) orientation: implications for diabody flexibility. J Mol Biol. 2003; 326:341–51. [PubMed: 12559905]
12. Li L, Bading J, Yazaki PJ, Ahuja AH, Crow D, Colcher D, Williams LE, Wong JY, Raubitschek A, Shively JE. A versatile bifunctional chelate for radiolabeling humanized anti-CEA antibody with In-111 and Cu-64 at either thiol or amino groups: PET imaging of CEA-positive tumors with whole antibodies. Bioconjug Chem. 2008; 19:89–96. [PubMed: 17988078]
13. Ruangma A, Laforest R, Bing B, Leahy RM. Characterization of USC-MAP image reconstruction on microPET-R4. Nuclear Sci Symp Conf Record. 2004; 6:3449.
14. Holliger P, Hudson PJ. Engineered antibody fragments and the rise of single domains. Nat Biotechnol. 2005; 23:1126–36. [PubMed: 16151406]
15. Robinson MK, Shaller C, Garmestani K, Plascjak PS, Hodge KM, Yuan QA, Marks JD, Waldmann TA, Brechbiel MW, Adams GP. Effective treatment of established human breast tumor xenografts in immunodeficient mice with a single dose of the alpha-emitting radioisotope astatine-211 conjugated to anti-HER2/neu diabodies. Clin Cancer Res. 2008; 14:875–82. [PubMed: 18245551]
16. Schneider DW, Heitner T, Alicke B, Light DR, McLean K, Satozawa N, Parry G, Yoo J, Lewis JS, Parry R. In vivo biodistribution, PET imaging, and tumor accumulation of 86Y- and 111In-

antimindin/RG-1, engineered antibody fragments in LNCaP tumor-bearing nude mice. J Nucl Med. 2009; 50:435–43. [PubMed: 19223400]

17. Leyton JV, Olafsen T, Sherman MA, Bauer KB, Aghanjanian P, Reiter RE, Wu AM. Engineered humanized diabodies for microPET imaging of prostate stem cell antigen-expressing tumors. Protein Eng Des Sel. 2009; 22:209–216. [PubMed: 18957406]
18. Cai X, Garen A. Comparison of fusion phage libraries displaying VH or single-chain Fv antibody fragments derived from the antibody repertoire of a vaccinated melanoma patient as a source of melanoma-specific targeting molecules. Proc Natl Acad Sci U S A. 1997; 94:9261–6. [PubMed: 9256470]
19. McCabe KE, Wu AM. Positive progress in ImmunoPET--not just a coincidence. Cancer Biother Radiopharm. 25:253–61. [PubMed: 20578830]
20. Sundaresan G, Yazaki PJ, Shively JE, Finn RD, Larson SM, Raubitschek AA, Williams LE, Chatziioannou AF, Gambhir SS, Wu AM. 124I-labeled engineered anti-CEA minibodies and diabodies allow high-contrast, antigen-specific small-animal PET imaging of xenografts in athymic mice. J Nucl Med. 2003; 44:1962–9. [PubMed: 14660722]
21. Behr TM, Becker WS, Sharkey RM, Juweid ME, Dunn RM, Bair HJ, Wolf FG, Goldenberg DM. Reduction of renal uptake of monoclonal antibody fragments by amino acid infusion. J Nucl Med. 1996; 37:829–833. [PubMed: 8965154]
22. Santos AD, Kashmiri SV, Hand PH, Schlom J, Padlan EA. Generation and characterization of a single gene-encoded single-chain-tetravalent antitumor antibody. Clin Cancer Res. 1999; 5:3118s–3123s. [PubMed: 10541352]
23. Chauhan SC, Jain M, Moore ED, Wittel UA, Li J, Gwilt PR, Colcher D, Batra SK. Pharmacokinetics and biodistribution of 177Lu-labeled multivalent single-chain Fv construct of the pancarcinoma monoclonal antibody CC49. Eur J Nucl Med Mol Imaging. 2005; 32:264–73. [PubMed: 15791435]
24. Wittel UA, Jain M, Goel A, Chauhan SC, Colcher D, Batra SK. The in vivo characteristics of genetically engineered divalent and tetravalent single-chain antibody constructs. Nucl Med Biol. 2005; 32:157–64. [PubMed: 15721761]
25. Goel A, Baranowska-Kortylewicz J, Hinrichs SH, Wisecarver J, Pavlinkova G, Augustine S, Colcher D, Booth BJ, Batra SK. 99mTc-labeled divalent and tetravalent CC49 single-chain Fv's: novel imaging agents for rapid in vivo localization of human colon carcinoma. J Nucl Med. 2001; 42:1519–27. [PubMed: 11585867]
26. Tempero M, Leichner P, Baranowska-Kortylewicz J, Harrison K, Augustine S, Schlom J, Anderson J, Wisecarver J, Colcher D. High-dose therapy with 90Yttrium-labeled monoclonal antibody CC49: a phase I trial. Clin Cancer Res. 2000; 6:3095–102. [PubMed: 10955789]
27. Alvarez RD, Huh WK, Khazaeli MB, Meredith RF, Partridge EE, Kilgore LC, Grizzle WE, Shen S, Austin JM, Barnes MN, Carey D, Schlom J, LoBuglio AF. A Phase I study of combined modality (90)Yttrium-CC49 intraperitoneal radioimmunotherapy for ovarian cancer. Clin Cancer Res. 2002; 8:2806–11. [PubMed: 12231520]
28. Meredith RF, Bueschen AJ, Khazaeli MB, Plott WE, Grizzle WE, Wheeler RH, Schlom J, Russell CD, Liu T, LoBuglio AF. Treatment of metastatic prostate carcinoma with radiolabeled antibody CC49. J Nucl Med. 1994; 35:1017–22. [PubMed: 8195861]
29. Beresford GW, Pavlinkova G, Booth BJ, Batra SK, Colcher D. Binding characteristics and tumor targeting of a covalently linked divalent CC49 single-chain antibody. Int J Cancer. 1999; 81:911–7. [PubMed: 10362138]
30. Pasut G, Veronese FM. PEGylation for improving the effectiveness of therapeutic biomolecules. Drugs Today (Barc). 2009; 45:687–95. [PubMed: 19956810]
31. Junutula JR, Flagella KM, Graham RA, Parsons KL, Ha E, Raab H, Bhakta S, Nguyen T, Dugger DL, Li G, Mai E, Lewis Phillips GD, Hiraragi H, Fuji RN, Tibbitts J, Vandlen R, Spencer SD, Scheller RH, Polakis P, Sliwkowski MX. Engineered Thio-TrastuzuMAb-DM1 Conjugate with an Improved Therapeutic Index to Target Human Epidermal Growth Factor Receptor 2-Positive Breast Cancer. Clin Cancer Res. 16:4769–4778. [PubMed: 20805300]

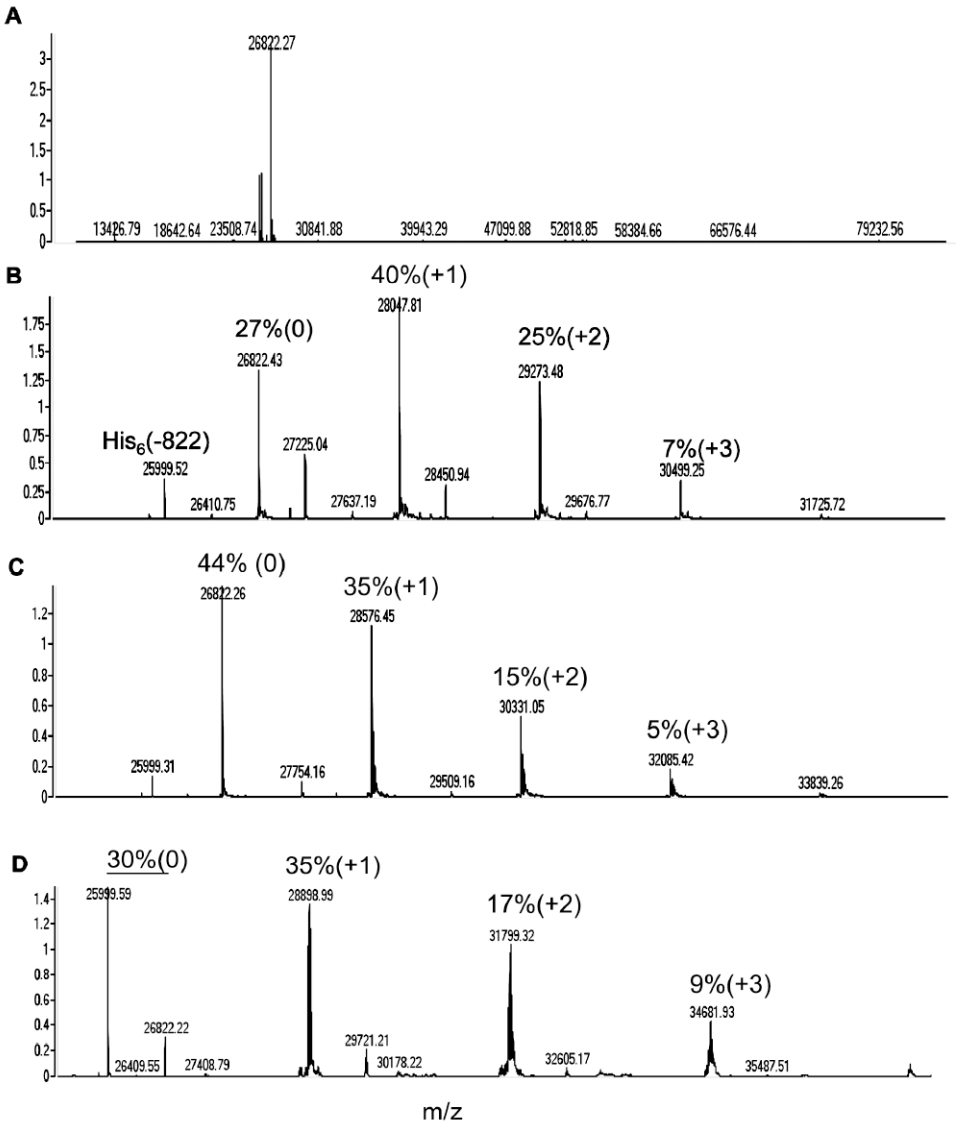

Figure 1. High resolution nanospray mass spectrometry analysis of PEGn AVP04-50 conjugates

A. Deconvoluted mass spectrum for non-PEGylated diabody (n= 0). **B**. Deconvoluted mass spectrum for PEG12 conjugate (n= 12). **C**. Deconvoluted mass spectrum for PEG24 conjugate (n= 24). **D**. Deconvoluted mass spectrum for PEG48 conjugate (n= 48). The percent peak height for unmodified (0), mono-derivative (+1), and di-derivatives (+2) are shown above the peaks. In the case of the PEG48 conjugate, the unmodified percent was summed for the parent mass (26, 822) and the parent mass minus the His-6 tag (25,999).

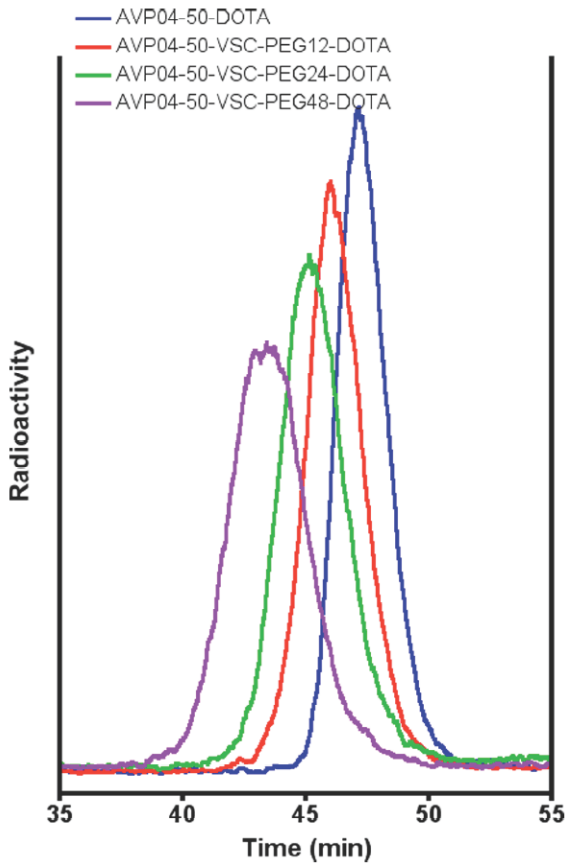

Figure 2. Size exclusion chromatography of radiolabeled uncojugated and PEGylated AVP04-50 diabody

All samples were radiolabeled with ^{111}In and run on a Superdex 75 size exclusion column as described in Methods (radioactivity in arbitrary units). Blue: DOTA- non-PEGylated diabody conjugate. Red: DOTA-PEG12-diabody conjugate. Green: DOTA-PEG24-diabody conjugate. Purple: DOTA-PEG48-diabody conjugate.

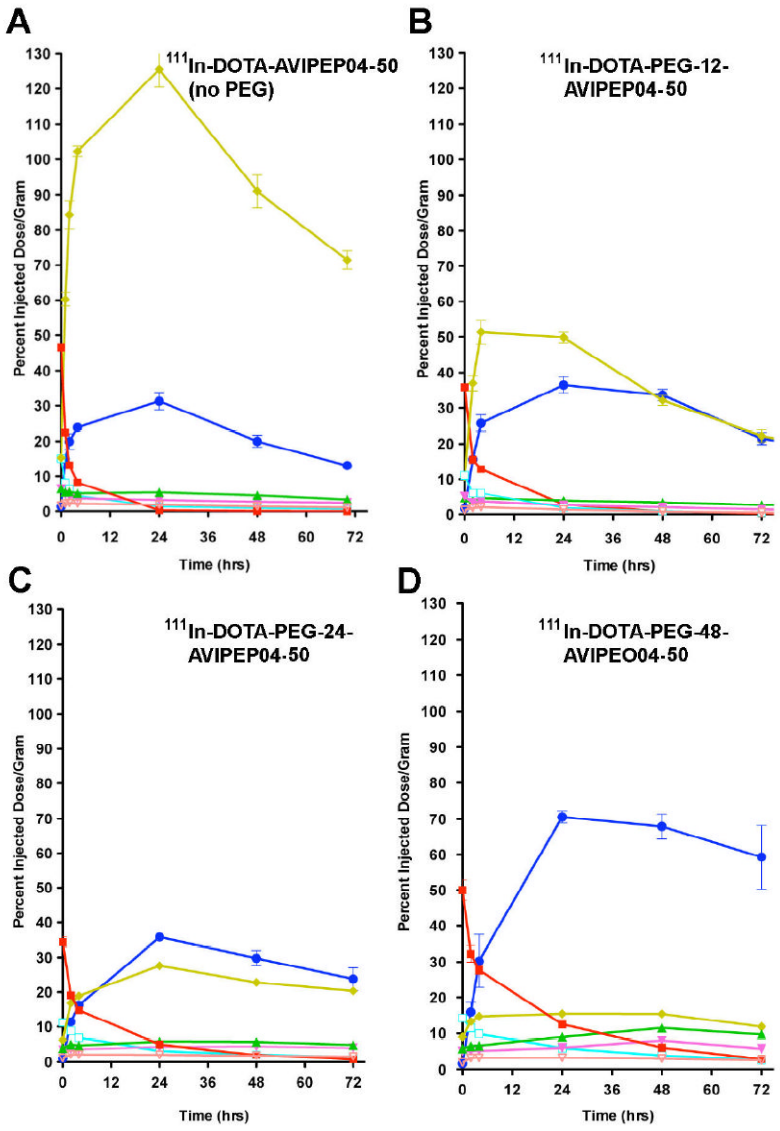

Figure 3. Biodistribution of DOTA-PEGn-AVP04-50 conjugates in athymic mice bearing LS-174T xenografts

The biodistribution of the constructs was determined in athymic mice bearing LS-174T xenografts as described in Methods. **A**. ^{111}In-DOTA-AVP04-50 (PEGn= 0). **B**. ^{111}In-DOTA-PEG12-AVP04-50 (PEGn= 12). **C**. ^{111}In-DOTA-PEG24-AVP04-50 (PEGn= 24). **D**. ^{111}In-DOTA-PEG48-AVP04-50 (PEGn= 48). Key: yellow= kidney, dark blue= tumor, red= blood, green= liver, light blue= lungs, magenta= spleen, orange= carcass.

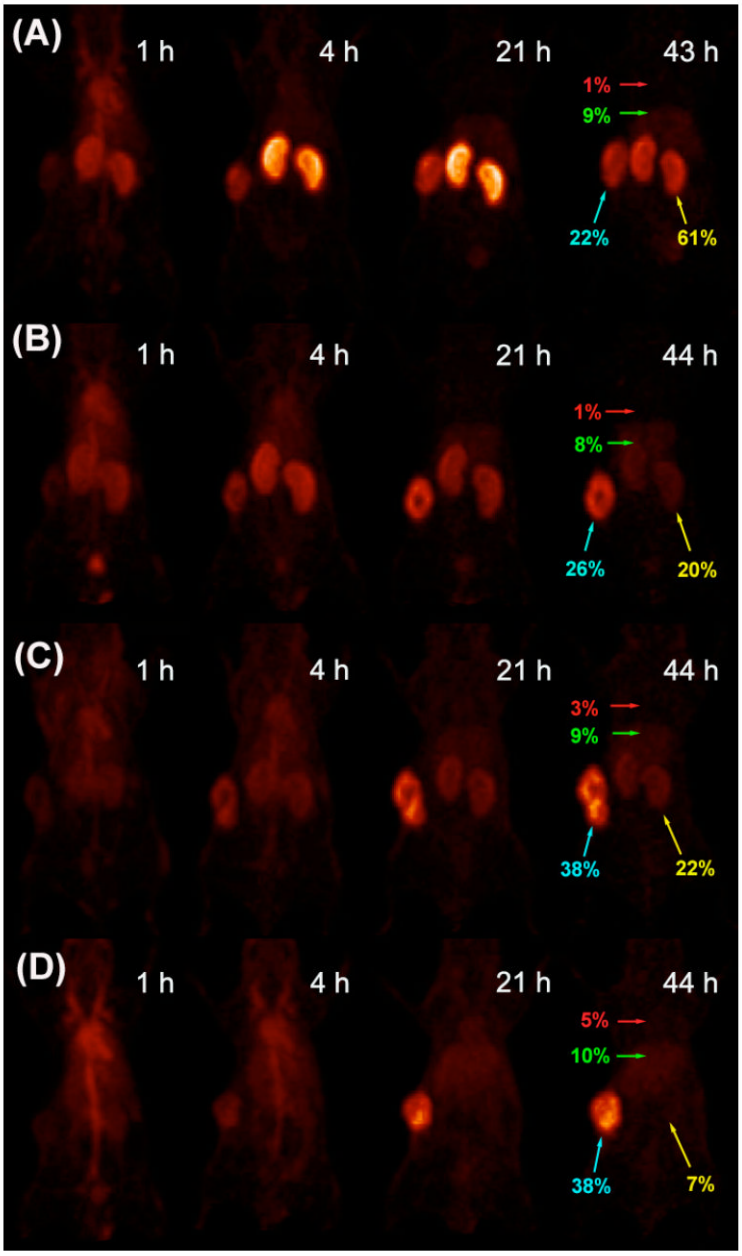

Figure 4. Serial PET imaging of ^{64}Cu-DOTA-PEGn-AVP04-50 in athymic mice bearing LS-174T xenografts

(**A**) PEG0, (**B**) PEG12, (**C**) PEG24 and (**D**) PEG48. Images are anterior-view maximum intensity projections (MIPs) normalized to reflect radiodecay-corrected relative image intensity per unit injected activity. Labels in red, green, yellow and turquoise respectively show %ID/g in blood (heart), liver, kidney and tumor as measured by direct assay following the final scan. Tumor weights at time of sacrifice were 314, 316, 382 and 341 mg in (A) - (D) respectively.

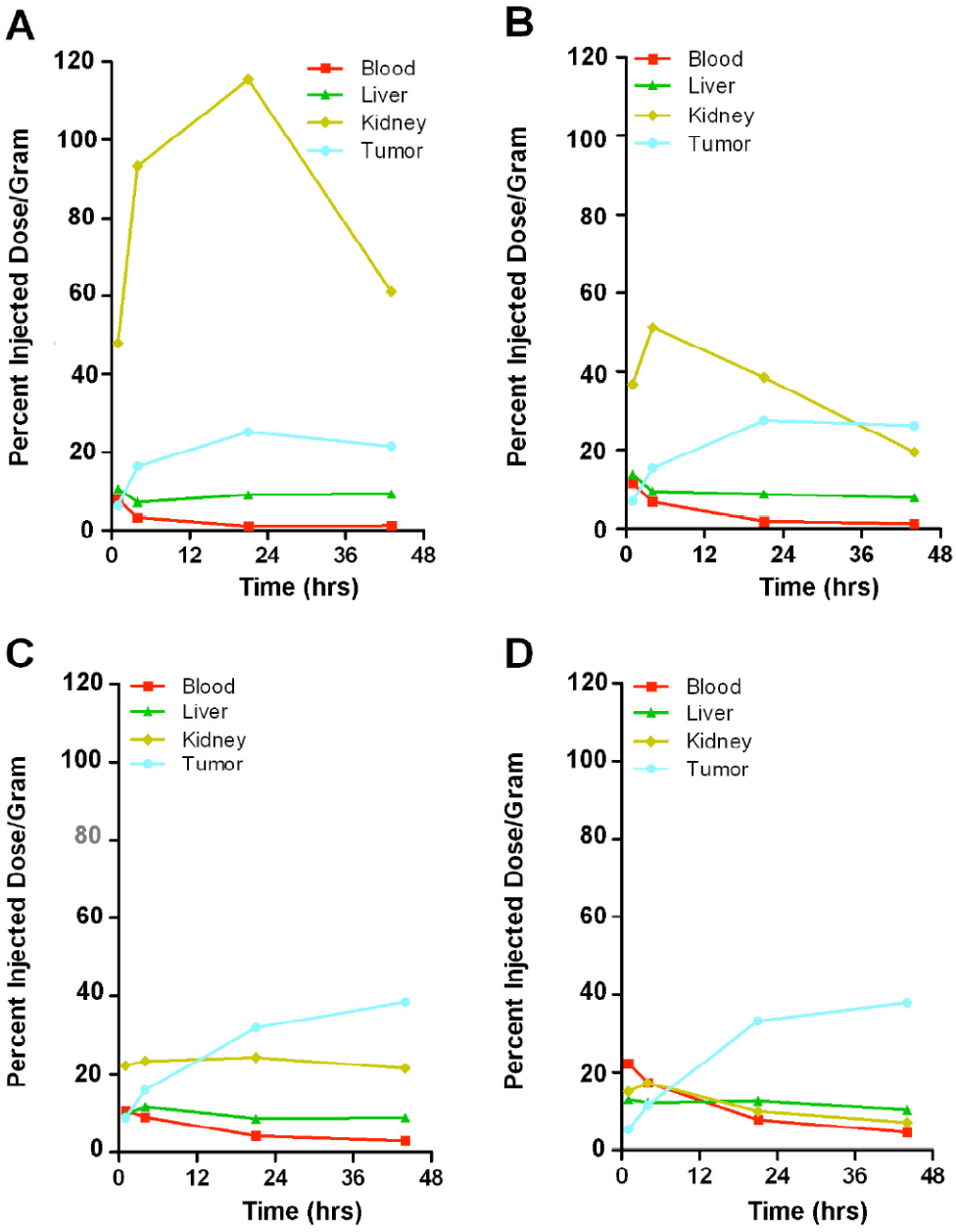

Figure 5. Time-activity curves derived from serial microPET studies depicted in Figure 4
A. PEG0. **B**. PEG12. **C**. PEG24. **D**. PEG48; 1 animal each).

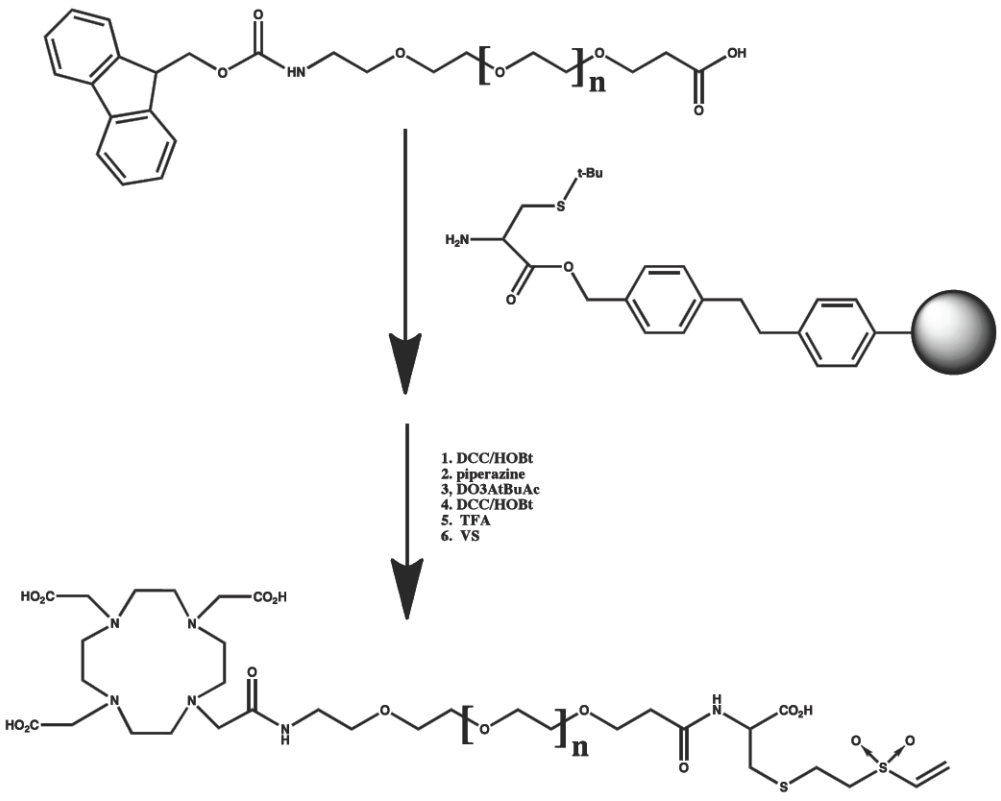

Scheme 1. Synthesis of DOTA-PEG-Cys-VS

FMOC-amido-PEG-acid was conjugated to S-t-butyl cysteine on Wang resin using standard activation chemistry (DCC/HOBt). The FMOC was removed with piperazine and conjugated to DO3AtBuAc using standard activation chemistry (DCC/HOBt). The product was removed from the resin with TFA, purified by reverse phase HPLC, reacted with excess vinyl sulfone in DMF, and repurified by reverse phase HPLC. N= 12 and 24. For N=48, PEG24 was coupled twice prior to addition of D03AtBu-Ac.